Biomass Conversion and Biorefinery (2024) 14:3523–3534
https://doi.org/10.1007/s13399-022-02614-x

ORIGINAL ARTICLE

Application of a biowaste of fish (*Labeo rohita*) scale for the removal of methyl orange from aqueous solutions: optimization of sorption conditions by response surface method and analysis of adsorption mechanism

Debabrata Nandi[1] · Harikrishnan Pulikkalparambil[1] · Jyotishkumar Parameswaranpillai[2] · Suchart Siengchin[1,3]

Received: 17 December 2021 / Revised: 16 March 2022 / Accepted: 17 March 2022 / Published online: 9 April 2022

Abstract

Methyl orange, an anionic dye, is injurious to health and the environment which must be treated before discharging. The processed fish (*Labeo rohita*) scales were characterized by scanning electron microscope (SEM), the attenuated total reflectance (ATR) Fourier transform infrared spectroscopy (FT-IR), and BET surface area analyzer. The BET surface area and pore diameter were observed to be 192 $m^2\ g^{-1}$ and 44 nm, respectively. Influences of parameters such as *pH*, temperature, and concentration of adsorbent were studied by response surface methodology and analysis of variance (ANOVA) to optimize methyl orange dye uptake in adsorption process by fish scale. The influences of factors on adsorption capacity followed the order (initial concentration > temperature > *pH*). The fish scale attained a high sorption capacity (Langmuir capacity of 520 mg g^{-1} at *pH* 5.3, 283 K) towards methyl orange. The thermodynamics analyses implied that the physisorption was an exothermic and spontaneous process (ΔG^0 = negative, $\Delta H^0 = -9.17$ kJ mol^{-1} and $\Delta S^0 = +0.03$ J $mol^{-1}\ K^{-1}$). The interaction of fish scale biosorbent with methyl orange dye was also explored with the assistance of a mechanistic pathway. The results indicate that the fish scale could be employed as an effective biosorbent for the removal of methyl orange dye from aqueous solution.

Keywords Adsorption mechanism · Biosorbent · Biowaste · Fish scale · Methyl orange

Highlights

Biosorbent was developed by HCl activation of *Labeo rohita* scale
Acid treatment generated pores on fish scale surface
RSM analysis optimized methyl orange dye adsorption by biosorbent
Maximum dye adsorption capacity was obtained ~520 mg/g
Physisorption-based mechanism was established

✉ Suchart Siengchin
suchart.s.pe@tggs-bangkok.org

[1] Department of Materials and Production Engineering, The Sirindhorn International Thai-German Graduate School of Engineering, King Mongkut's University of Technology North Bangkok (KMUTNB), 1518 Pracharat 1 Road, Bangkok, Bangsue 10800, Thailand

[2] Department of Science, Faculty of Science & Technology, Alliance University, Chandapura-Anekal Main Road, Bengaluru, Karnataka 562106, India

[3] Center of Innovation in Design and Engineering for Manufacturing, King Mongkut's University of Technology North Bangkok, 1518 Pracharat 1 Road, Bangkok, Bangsue 10800, Thailand

1 Introduction

In this modern era, dyes are widely used in textiles, printing, cosmetics, rubber, paper, food, leather, and pharmaceutical industries to color their products [1]. These industries generate color effluents that are exceedingly toxic to the environment. These dyes can damage aquatic life and organs of human beings as well as exhibit negative effects on photosynthesis [2]. Due to its complex structure and water solubility characteristics, dye removal from effluent is very tough by means of conventional physicochemical methods, such as membrane filtration, coagulation, chemical oxidation, chemical precipitation, and osmosis [3]. Moreover, most dyes are inactive towards environmental conditions, such as microbial interaction, heat, and light [4]. Therefore, researchers have paid considerable attention to optimize removal solutions of dyes from aqueous medium [5, 6]. However, the adsorption process endows the capability of dye removal with remarkable advantages over other conventional methods, such as simplicity, high efficiency, low treatment cost, low sludge

generation, and non-generation of toxic materials. Among the reactive dyestuffs, methyl orange (MOH) is photo-physically and chemically inactive and may be responsible for respiratory tract malfunction, allergic dermatitis, eye irritation, gastrointestinal irritation with vomiting, diarrhea, and nausea [7, 8]. The MOH is chosen here on account of its use in printing papers, food, textiles, research laboratories, and pharmaceutical industries. The abundant availability of biomass makes it an eco-friendly and economically viable material to apply in numerous fields [9], including adsorption. Sometimes, easy activation of biomass is a key strategy to turn it into a promising adsorbent, as reported by Niero et al. [10]. *Sardinella brasiliensis* scale, *Catla catla* scale, fish scale chitin, etc. were utilized as promising adsorbents for dye removal [10–13].

The present work is an attempt to explore the possibility of utilizing bio-based waste materials, *Labeo rohita* fish scale, as an adsorbent to assess the adsorption behavior for the removal of the most common and well-known dye, methyl orange. The cycloid scales are uniform and contain generally 41% protein, 13% lipid, and 15% ash, the balanced consisted (31%) nitrogen-free extract containing carbohydrate, etc. [14]. As the fish scale contains protein, it might be a potential immobilizer of unsafe chemicals from the environment due to the capability of proteins to chelate heavy metal ions, as similarly reported by Tamás et al. [15]. Moreover, acid treatment on the fish scale makes its surface uneven and porous, which is an additional advantage for the adsorption of adsorbate species. So, the adsorption behavior of the fish scale towards methyl orange on physicochemical aspects was systematically assessed with insight into the proposed mechanism. The $-NH_2$ and $^{>}NH$ groups of amino acids were illustrated to interact with the $-SO_3^-$ group of methyl orange dye. The influence of temperature, adsorbent dose, contact time, and sorbate concentration was investigated to explore the removal efficiency and reaction pathway of methyl orange adsorption from aqueous solution.

2 Materials and methods

2.1 Materials and analytical tools

Methyl orange ($C_{14}H_{14}N_3SO_3H$), an anionic dye, was utilized as received. A stock solution of MOH (1000 mg L^{-1}) was prepared and diluted as per the initial concentration requirement. A ELICO India (model: LI) *pH* meter was used for analysis. The scanning electron microscope (SEM) of JEOL, Japan (model: JSM 6390LV), was used for morphology analysis. An N_2 (gas) adsorption-desorption isotherm was tested to study BET surface area and porosity (Quantachrome Autosorb-1C surface analyzer). The attenuated total reflection (ATR) Fourier transform infrared spectroscopy (FT-IR) study was performed within the range of 4000 to 650 cm^{-1} wavenumber by 500 cm^{-1}/min scan rate, purchased from PerkinElmer, USA. The UV/vis spectrophotometer (HITACHI, model U-3210) was used to determine dye concentration at 464 nm. The color of methyl orange is associated with the presence of certain groups in the molecules called "chromophores," and the color is augmented by the presence of certain groups called "auxochromes." The group $-SO_3H$ is unable to produce color itself but can deepen the color produced by the azo group (−N=N−) in the dye. Dye (methyl orange) = chromophore (azo group) + auxochrome ($-SO_3H$) [16]. The physical characteristics of MOH were presented in Table S1 (S = supporting information). In supporting information section, MOH solution preparation and its spectrophotometric estimation were presented.

Fig. 1 Pathway of biosorbent preparation and activation by acid treatment

2.2 Preparation of biosorbent

The fish scale was collected, ground finely, and cleaned very carefully by washing with distilled water and ethanol several times. It was treated with 0.1 M HCl for 3 h and afterward washed thoroughly with distilled water to remove excess acid. This acid-treated fish scale (Fig. 1) was dried in an air oven at 80–100 °C for 3 h. Thereafter, the mesh size of the fish scale collected was ranged from 25 to 50 µm for use in adsorption study.

2.3 Batch adsorption

A 50-ml aliquot of MO-H with 0.2 g of adsorbent was taken into a 100 ml well-capped polyethylene bottle for

mechanical agitation. The adjusted solution *pH* was~5.3 by 0.1M HCl/NaOH. The agitation (shaking) speed used was of 300 ± 5 rpm. The filtered solution was used to determine the concentration of unreacted dye. The adsorption capacity q_e (mg/g) of MO-H was determined [17] by Eq. (1):

$$q_e = \left(C_0 - C_e\right)\mathrm{V/m} \tag{1}$$

where m (g) is the mass of adsorbent, V (L) is the volume of MOH solution, and C_0 and C_e (mg/L) are the initial and equilibrium concentration of MOH solution, respectively. The influence of *pH* on the adsorption of MO-H by fish scale was tested in the *pH* range between 2 and 10, adjusted initially (pH_i) by acid/base at 303 K. The agitation time was fixed at 2 h as this effect was investigated initially. The scale size and agitation speed used were mentioned above.

This kinetic study was done at *pH* 5.3 (± 0.1) at 283 K, 303 K, and 323 K with a fluctuation of ± 1.0 K. Here, 500.0 ml of 200 mg L^{-1} MO-H solution was mixed with 2.0 g of scale in a bottle and kept in a thermostat bath to reach anticipated temperature. The agitation speed was fixed at 300 ± 5 rpm. A definite volume of 2 ml was collected at 5.0-min intervals from the start to the point of equilibrium in a 50 ml beaker. Afterward, the solution was transferred to a 25 ml volumetric flask and made up the volume with distilled water for analysis by spectrophotometer. To comprehend the adsorption phenomenon along with process optimization and efficient utilization of the adsorbent, the adsorption data was kinetically analyzed by kinetic model equations.

The pseudo-first-order and pseudo-second-order Eqs. (2) and (3), respectively [18], were used to fit kinetic data:

$$q_t = q_e\left\{1 - \exp\left(k_1 t\right)\right\} \tag{2}$$

$$q_t = k_2 q_e^{\,2}\, t/\left\{1 + \left(k_2 qt\right)\right\} \tag{3}$$

where q_t reflects adsorption capacity (mg g^{-1}) at time *t*, q_e shows the same (mg g^{-1}) at equilibrium point, K_1 signifies the rate constant (min^{-1}) for pseudo first order, and K_2 reflects the rate constant (mg g^{-1} min^{-1}) for pseudo-second-order equation at time *t* (min).

The equilibrium studies were performed by the batch method at 283 K, 303 K, and 323 K (*pH*~5.3 ± 0.1). The concentration of MO-H solution used in the study ranged from 40.0 to 320.0 mgL^{-1}. The dose of the adsorbent was 0.4 g made for 100 ml of MO-H. The agitation time was set for 2 h at 300 ± 5 rpm speed. After reaching equilibrium, the solution was filtered, and the *pH* was adjusted to 5.3 (± 0.1) to be analyzed by a spectrophotometer. The isotherm equilibrium data obtained by batch method were analyzed using the isotherm model equations, Langmuir [19], Freundlich [20], and Redlich-Peterson [21] isotherm Eqs. (4, 5, and 6):

$$q_e = \frac{q_m K_a C_e}{1 + K_a C_e} \tag{4}$$

$$q_e = K_f C_e^{\,1/n} \tag{5}$$

$$q_e = \frac{\alpha C_e}{1 + \beta . C_e^{\gamma}} \tag{6}$$

where *n* denotes sorption intensity, K_f represents Freundlich constant, q_e (mg g^{-1}) represents the amount of MOH sorption, K_a represents the Langmuir constant (L mg^{-1}), C_e (mg L^{-1}) shows the concentration at equilibrium point, q_m shows the monolayer adsorption capacity (mg g^{-1}), and α, β, and γ ($0 < \gamma < 1$) are the three isotherm constants which illustrate the feature of the isotherm, respectively.

The parameters associated with thermodynamic study were illustrated by Eqs. (7–9) [22]:

$$\Delta G^0 = -RT\ \ln\ b \tag{7}$$

$$\ln \frac{b_1}{b_2} = -\frac{\Delta H^0}{R}\left(\frac{1}{T_1} - \frac{1}{T_2}\right) \tag{8}$$

$$\Delta G^0 = \Delta H^0 - T\Delta S^0 \tag{9}$$

where *b* be the constant in L mol^{-1}, $R = 8.314$ J mol^{-1} K^{-1}, i.e., the ideal gas constant, ΔG^0 (Gibbs-free energy),ΔH^0 (standard enthalpy), and ΔS^0 (standard entropy) are in J mol^{-1}, J mol^{-1}, and J mol^{-1} K^{-1}, respectively.

3 Results and discussion

The results of SEM and BET studies described the influence of surface morphology on the adsorption of MO-H on fish scale. The results reported herein were the influences of *pH*, contact time for kinetics at different temperatures, initial different adsorbent doses, and equilibrium studies with varying concentrations of MO-H. The affinity of the dye towards biosorbant is demonstrated by a mechanistic pathway.

3.1 SEM, BET surface area, and FT-IR analysis

The surface characterization of fish scale is shown in Fig. 2. The SEM micrographs in Fig. 2a and b reveal the clear, distinct porous morphology of the processed scales. The preparation pathway along with acid treatment of biosorbant helps to generate pores during the elimination of organic/inorganic compounds. These exposed pores quickly allow adsorbate

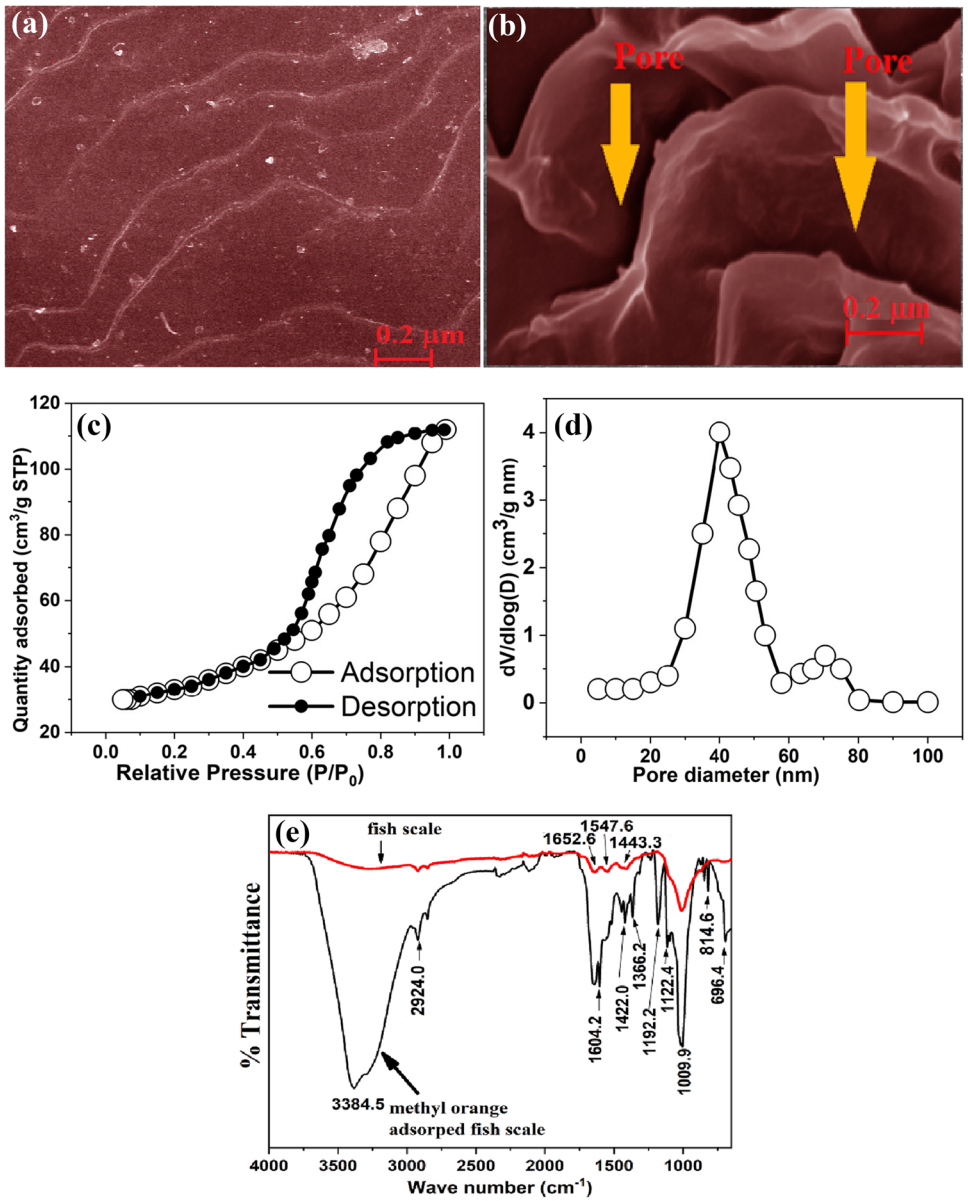

Fig. 2 SEM images of fish scale **a** before acid treatment, **b** after acid treatment, BET **c** adsorption-desorption isotherm of N_2 gas on fish scale, **d** pore-size distribution on fish scale surface, and **e** ATR FTIR analysis of pure fish scale and methyl orange adsorbed fish scale

to be entrapped on their surface. The BET surface area and pore volume are 190 $m^2\ g^{-1}$ and 0.23 $cm^3\ g^{-1}$, respectively. This specific surface area is high enough to accommodate MOH molecules on the active surface of biosorbent. The Langmuir surface area is 236 $m^2\ g^{-1}$, which is higher than the BET surface area value. Here, Langmuir surface area is based on monolayer adsorption of an adsorbate which is not absolutely real for freely accessible surface because there will be lateral interactions among adsorbate molecules as well as different affinity of the adsorbate molecules towards the adsorbent. The average pore diameter is 44 nm, which reveals its mesoporous structure. The hysteresis loop in Fig. 2c isotherm belongs to type IV, which is also associated with the mesoporous structure. The size of the MOH is 1.2 nm [23], while the pore diameter is 44 nm (Fig. 2d). Thus, the pores can easily accommodate many adsorbates, i.e., MOH molecules on their active surface sites from the bulk phase of the dye solution. The significance of the mesoporosity in dye removal was also explored by Hadi et al. [24] on activated carbon. Figure 2e shows the FT-IR spectrum of fish scale before and after dye adsorption. The band at 2924.0 cm^{-1} for both fish scale and dye-adsorbed fish scale is owing to the asymmetric $-CH_3$ stretching vibration [25]. The bands at 1443.3 cm^{-1}, 1547.6 cm^{-1}, and 1652.6 cm^{-1} endorse the integrity of the proteins inside the fish scale. The bands at 1422.0 cm^{-1} and 1604.2 cm^{-1} are characteristics of in-plane C–H bending (−C=C–H) and −N=N stretching of the methyl orange dye molecule, respectively. The band at 1366.2 cm^{-1} corresponds to the −S=O stretching vibration, which confirms the presence of sulfonic group in the dye.

Table 1 Parameters listed from analysis of variance (ANOVA) for quadratic model

Source	Sum of squares	Degree of freedom	Mean square	*F*-value	*p*-value	Coefficient
Model	56763.64	9	6307.07	9.49	0.0008	115.80 (intercept)
A-Temp	7583.33	1	7583.33	11.41	0.0070	−23.56
B-pH	0.1551	1	0.1551	0.0002	0.9881	−0.1066
C-Ci	31680.79	1	31680.79	47.65	< 0.0001	48.16
AB	175.78	1	175.78	0.2644	0.6183	4.69
AC	442.53	1	442.53	0.6656	0.4336	−7.44
BC	205.03	1	205.03	0.3084	0.5909	−5.06
A^2	993.72	1	993.72	1.49	0.2495	+8.30
B^2	13474.51	1	13474.51	20.27	0.0011	+30.58
C^2	4322.87	1	4322.87	6.50	0.0289	+17.32

The bands at 1122.4 cm^{-1} and 1192.2 cm^{-1} are characteristics of the −C–N bond, which confirms the presence of an azo group in the dye. In dye-adsorbed fish scale, the band at 814.6 cm^{-1} is characteristic of distributed benzene ring, which supports the aromatic nature of the dye. The band at 696 cm^{-1} corresponds to −C–S stretching vibration, which is presumably due to the presence of dye in the fish scale.

3.2 Methyl orange adsorption study

3.2.1 Response surface methodology and ANOVA study

This optimization study was performed by the central composite design method in Design-Expert 9 (DX9) software [26]. Twenty different experiments were run with three independent variables as shown in Table S2. The effect of parameters such as temperature (T), pH, and initial concentration of the adsorbate (C_i) on response, i.e., adsorption capacity (q, mg/g), were investigated and summarized in Table 1. High and low values were set as per the scale-up of the adsorption phenomenon. The experimental results were fitted with second-order polynomial model Eq. (10):

$$y = \beta_0 + \sum_{i=1}^{3} \beta_i x_i + \sum_{i=1}^{3} \beta_{ii} {x_i}^2 + \sum_{i=1}^{3} \sum_{j=i+1}^{3} \beta_{ij} x_i x_j \quad (10)$$

where y is the response, x is an independent variable, β_0 is the constant coefficient, β_i is the linear coefficient, β_{ii} is the quadratic coefficient, and β_{ij} is the ij interaction coefficient. The positive coefficient values reveal synergistic effects, whereas negative values reveal antagonistic effects of parameters on adsorption either for individual or in combination as shown in Eq. 11 [27].

$$\begin{aligned}\text{Adsorption capacity (mg/g)} = {} & 115.8 - 23.56\,A - 0.1066\,B + 48.16\,C \\ & + 8.30\,A^2 + 30.58\,B^2 + 17.32\,C^2 \\ & + 4.69\,AB - 7.44CA - 5.0BC\end{aligned} \quad (11)$$

Here factor A (temperature) shows an antagonistic effect, whereas factors B (pH) and C (C_i) express progressive effects on adsorption capacity as shown in the following Eq. (11). The regression coefficient (R^2) is 0.90, indicating models are fit best for factors or parameters. The small difference (0.1) between (R^2) and R^2 (Adj) signifies its close agreement between predicted and experimental adsorption capacity. The coefficient of factor B (pH) is very low negative, and with the rise of pH, the adsorption capacity increases rapidly up to pH 4 and then again decreases rapidly from pH 7.5 to 9. ANOVA can determine the significance of models. The F-value is 9.49, which implies the model is significant, and P-values are less than 0.05, which implies the model terms have a significant effect on the adsorption phenomenon. The higher the value of the coefficient, the greater its influence on the adsorption process which follows the order $Ci > T > pH$. This order can be attributed to the fact that the adsorption process primarily takes place between the adsorbent and adsorbate, so the adsorbate concentration (C_i) has a great influence on the adsorption process. However, the adsorption capacity decreases remarkably with a small rise in temperature, indicating physisorption type interaction which is also comparable with the thermodynamic study. On the other hand, the influence of pH change on adsorption capacity is the least which can be corroborated with the obtained results in the pH effect study. Figure 3a, b and c shows the plots of 3D responses where the MOH adsorption capacity is plotted against two parameters, keeping the other constant. Figure 3d exhibits standardized effects on adsorption where color points reflect in terms of normal %. It shows that most points are very close to the normal line, which implies that the model setup is substantial to describe the factor-dependent response. The dye adsorption capacity increased with the increase of C_i due to the opening of more accessible interaction sites, but the negative coefficient of temperature factor implies that the reaction is exothermic, which is corroborated by the values obtained from the

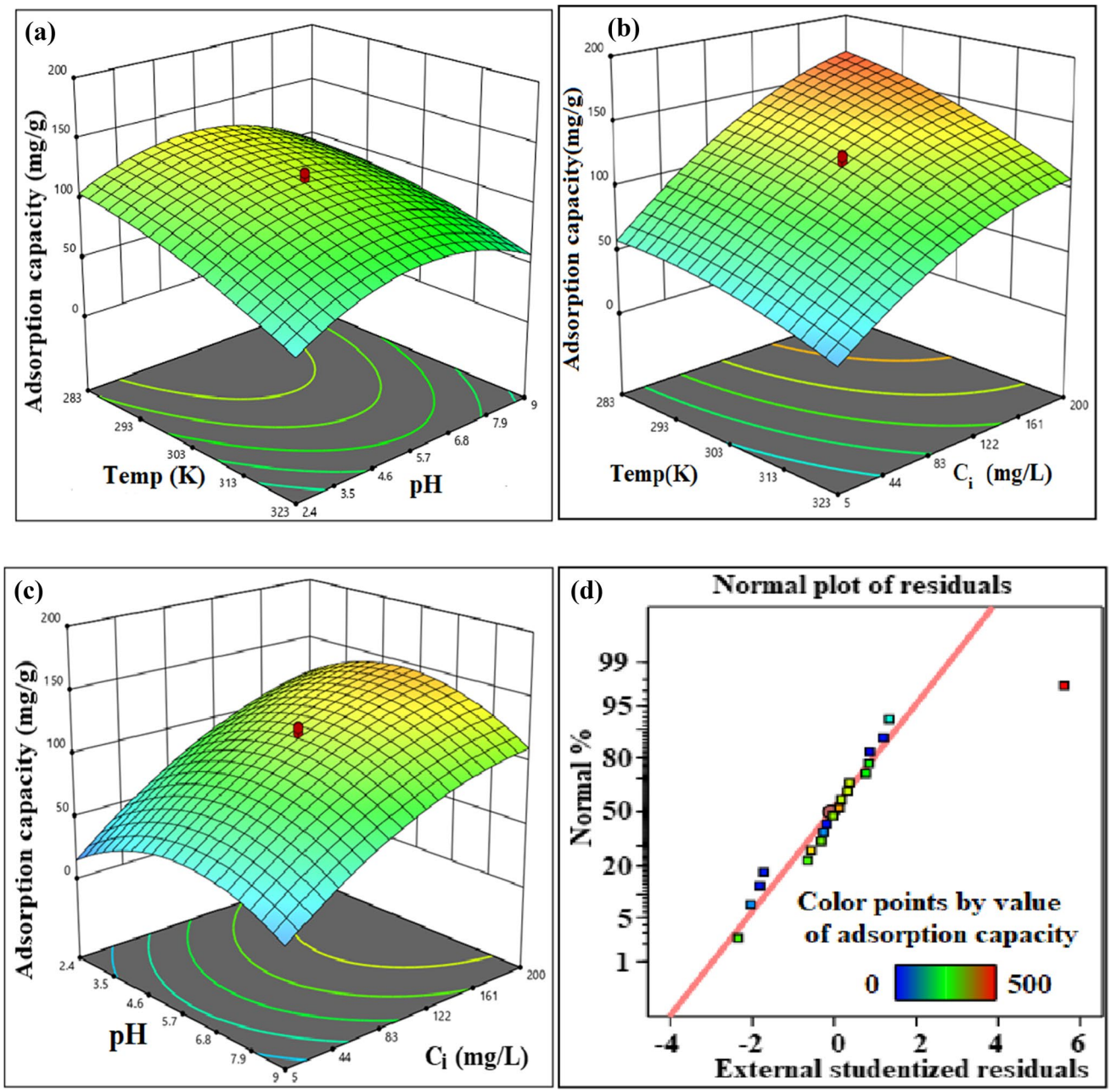

Fig. 3 Three-dimensional response surface plot interaction. **a** Influence of temperature (T) and *pH*, **b** influence of temperature and C_i and T, **c** influence of C_i and *pH*, and **d** color points by value of adsorption capacity in terms of normal plot of residuals

thermodynamic study. On the other hand, at lower *pH*, the adsorbent (fish scale) surface becomes protonated and delivers an electrostatic attraction between the adsorbent surface and dye molecule. According to *pK* value, the MO-H exists in the *pH* range (3.5 to 7.0) as MO^-, and the surface of the fish scale remains positively charged. So, the electrostatic attraction is assumed to be the source of binding force for MO^- in the adsorption process onto the positive surface of the fish scale.

3.2.2 Effect of pH

The adsorption range of MO-H is governed by solution *pH*. The *pH* dependence of dye adsorption onto biosorbent (S-NH_2) was investigated within 2.0 to 10.0 *pHi* using 200 mgL^{-1} initial concentration of MO-H with fixed adsorbent dosage where the adsorbent exhibits a *pH*-dependent surface charge (Fig. 4a). The results show that the MO-H adsorption increases from *pH* 2.0 to 3.5, remains nearly

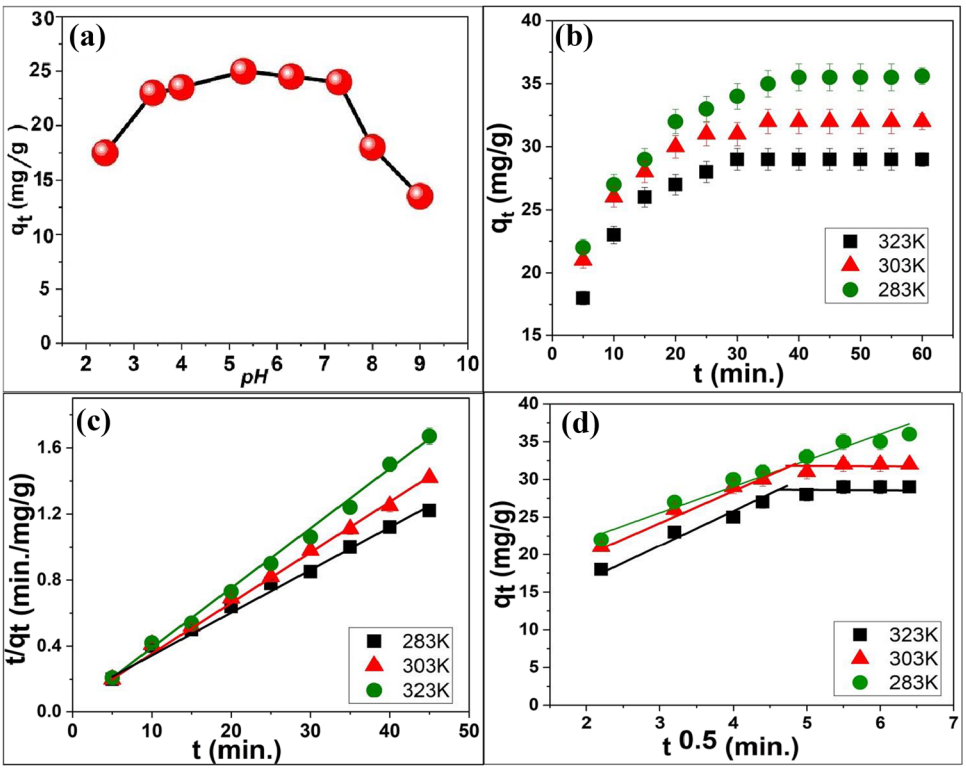

Fig. 4 **a** Effect of 2.0 to 10.0 *pH* on MO-H adsorption by fish scale. **b** Plot of q_t versus t of MO-H adsorption kinetic data on fish scale, C_i of MO-H: 200 mg L^{-1}, *pH* 5.3 (± 0.1). **c** The pseudo-second-order plot of MO-H adsorption kinetic data on fish scale at *pH* 5.3 (± 0.1). **d** Intraparticle diffusion plot for MO-H adsorption on fish scale for three different temperatures

constant up to *pH* 7.0, and then decreases with increasing *pH* from 7.0 to 10.0. The overall *pH*-dependent phenomenon is described stepwise by the proposed mechanism in Eqs. (12–14):

$$\text{(i) S-NH}_2 + \text{MO}^-_{(aq)} + \text{H}^+_{(aq)} \leftrightarrow \text{S-NH}_3^+ \text{--------} \overset{\text{H}}{\underset{|}{\text{O}}}\text{-M (at pH~2.0 to 3.5), [M = -C}_{14}\text{H}_{14}\text{N}_3\text{SO}_2\text{]}, \quad (12)$$

$$\text{(ii) S-NH}_2 + \text{MO}^-_{(aq)} + \text{H}^+_{(aq)} \leftrightarrow \text{S-NH}_3^+ \text{--------- O}^-\text{-M (at pH~3.5 to 7.0)}, \quad (13)$$

$$\text{(iii) S-NH}_2 + \text{MO}^-_{(aq)} + \text{OH}^-_{(aq)} \leftrightarrow \text{S-N}\begin{matrix}\text{H}\cdots\bar{\text{O}}\text{H}\\ \text{H}\cdots\bar{\text{O}}\text{H}\end{matrix} + \text{MO}^-_{(aq)}\,\text{(at pH > 7.0)}. \quad (14)$$

where S-NH_2 represents the fish scale surface which has some amine (–NH_2)-containing groups.

The phenomenon can be attributed to the protonation (H^+) at lower *pH* on the adsorbent (fish scale) surface, which arranges for a significant electrostatic attraction between the adsorbent surface and dye molecule as revealed in Eq. 12. Thus, the optimum range of *pH* for MO-H adsorption is found to be 3.5 to 7.0, which is pronounced by Eq. 13. According to *pK* value, the MO-H exists in the *pH* range (3.5 to 7.0) as MO^-, and the surface of the fish scale remains positively charged. So, the electrostatic attraction is assumed to be the source of the binding force of MO^- for the adsorption onto the positive surface of the biosorbant. After *pH* 7.0, a competition between hydroxyl (OH^-) ions and anionic dye molecules (MO^-) takes place, and consequently, the high mobility of hydroxyl (OH^-) ions towards adsorption sites inhibits dye adsorption. Thus, the adsorption capacity gradually decreases over pH 7.0 which is illustrated by Eq. 14 [28].

Table 2 Parameters obtained from kinetic study for MO-H adsorption onto fish scale at three different temperatures

Kinetic equation	Parameters	283 K	303 K	323 K
Pseudo first order	k_1 (min^{-1})	8.59×10^{-2}	14.26×10^{-2}	16.37×10^{-2}
	q_e (mg g^{-1})	24.18	22.23	30.11
	R^2	0.96	0.98	0.97
Pseudo second order	k_2 (mg $g^{-1}min^{-1}$)	4.87×10^{-3}	11.65×10^{-3}	23.97×10^{-3}
	q_e ($mg^{-1}g^{-1}$)	40.32	33.3	28.49
	R^2	0.99	0.99	0.99

3.2.3 Effect of fish scale dose

Figure S2 shows that with the rise of the dose of the adsorbent, the percentage of color removal is gradually increased, and for 1g of adsorbent, it becomes saturated which is similar to the reported results by Buema et al. [29]. For 1 g of adsorbent dose, the % of color removal is highest (93.8 %).

3.2.4 Kinetic study

The different adsorption capacities (q_t, mg g^{-1}) for MO-H in the adsorption reactions by fish scale at *pH* 5.3 (±0.1), with increasing contact time (t, min), are shown in Fig. 4b. The times needed to reach equilibrium of adsorption reaction at 283 K, 303 K, and 323 K are 45 min, 35 min, and 30 min, respectively. The stated parameters have been calculated using the slopes and intercepts of the linear plots of the pseudo-first-order and pseudo-second-order kinetic equations and are shown in Table 2. It is observed that the pseudo-second-order model equation fits better ($0.99 < R^2 < 1.0$) (Fig. 4c) than that of the pseudo-first-order equation ($0.96 < R^2 < 0.98$) (Fig. S3), and the pseudo-second-order model can substantially describe the kinetic nature of the adsorption reaction. Here, k_2 and the adsorption capacities (q_e, mg g^{-1}) of MO-H obtained here are found to increase and decrease, respectively, with the increase of temperature. The decrease in q_e with increasing temperature indicates the MO-H adsorption onto the fish scale is of an exothermic nature.

3.2.5 Diffusion kinetics

To predict the rate of adsorption reaction, the diffusion model was used by many researchers (Allen et al., 1989) as follows:

$$q_t = k_{id}\, t^{0.5} + C \tag{15}$$

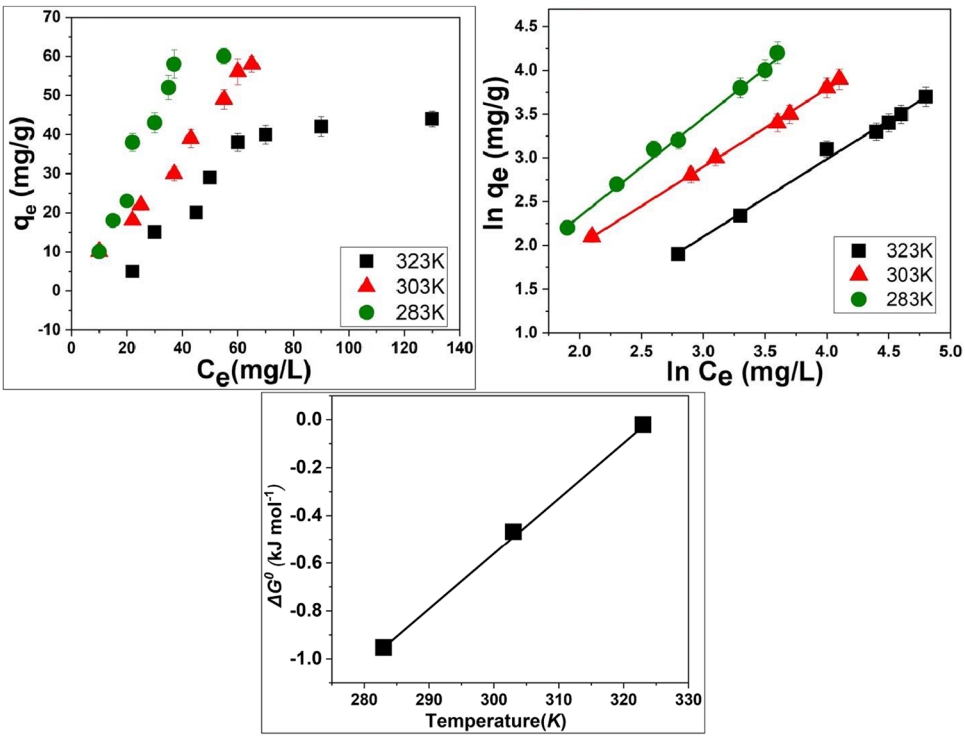

Fig. 5 **a** Plot of C_e versus q_e for MO-H adsorption on fish scale at *pH* 5.3 (± 0.1). The Freundlich isotherm fitting plot of MO-H adsorption equilibrium on fish scale at *pH* 5.3 ± 0.1. **c** Plot of ΔG^0 versus temperature of MO-H adsorption onto the fish scale at *pH* 5.3 (± 0.1)

where k_{id} (mg g^{-1} $min^{-0.5}$) describes the intraparticle diffusion rate constant and *C* describes film thickness as well as boundary layer effect calculated from intercept. Sorption process is a multistep process and the rate-limiting step, may be layer diffusion or pore diffusion controlled [30]. The plot of q_t versus $t^{0.5}$ is shown in Fig. 4d. The nonlinearity of the points at temperatures of 303 K and 323 K suggests the adsorption reactions rates are composed of two segments, which are almost straight lines associated with different slopes. At the initial stages, the q_t values sharply increase with time, which indicates film or boundary layer diffusion takes place at this stage, and at the latter stage, a horizontal portion is obtained, indicating pore diffusion predominates, which is corroborated with the pores shown in Fig. 2d. But at 283 *K*, it shows one linear segment, which indicates that the rate-determining step is governed by the layer diffusion. This can be ascribed by the transport of adsorbate molecules from bulk solution to the exterior surface of an adsorbent through a liquid film or layer.

3.2.6 Isotherm study

The isotherm data (Fig. 5a) for the adsorption of MO-H by fish scale at different temperatures is evaluated by linear regression using different adsorption model equations. Figure 5b, Fig. S4, and Fig. S5 show linear analysis of Freundlich isotherm, Redlich-Peterson isotherm, and Langmuir isotherm, respectively. The isotherm analyses of MO-H adsorption equilibrium data for fish scale indicate that the present data has been defined best using the Freundlich isotherm. The Redlich-Peterson isotherm (three-isotherm parameter equation) and the Langmuir isotherm (two-isotherm parameter equation) are equally followed at all the three studied temperatures. The equilibrium data fit parameters are shown in Table 3, which demonstrate the Freundlich model as the best fit, indicating the MO-H adsorption onto fish scale does not predominantly take place by monolayer, but the surface coverage is theoretically increased with the rise of the concentration of adsorbate. Freundlich constants "*n*" are found to lie within 0.96 to 1.28, suggesting a high adsorption capacity. The R^2 value, required to best describe the Redlich-Peterson model, is 0.91, which is far away from unity, indicates that the MO-H adsorption onto the fish scale takes place through multilayer process. Here, the Freundlich model is a better fit as its R^2 value (0.95) is a little higher than that of the Langmuir model fit (0.93), but their R^2 values are close to 1.0 indicating that both can describe the adsorption phenomenon. The Langmuir capacity is 520 mg g^{-1}, which is notable compared to the previous reports (Table 4). This finding suggests that the fish scale is a promising adsorbent for MO-H adsorption from aqueous solution.

Table 3 Parameters obtained from the analysis of the isotherm model equations at $pH = 5.3 \pm 0.1$ at three different temperatures

Isotherm models	Parameters	283 K	303 K	323 K
Freundlich	K_F	1.50	1.11	0.92
	n	0.97	1.06	1.27
	R^2	0.95	0.97	0.98
Langmuir	q_m (mg g^{-1})	520.32	85.47	89.28
	Ka (L mg^{-1})	2.78	0.01	0.01
	R^2	0.93	0.95	0.94
Redlich-Peterson	α	0.68	0.90	1.81
	β	0.01	0.02	0.02
	R^2	0.91	0.95	0.94

Table 4 Comparison of MO-H adsorption capacity of some reported adsorbents

Adsorbent	*T* (K)	Adsorption capacity (mg g^{-1})	Ref.
Graphene oxide	303	0.1	[31]
AC/Fe_2O4	293	20	[32]
Camel thorn plant	293	21	[33]
Cocoa pod husk	298	27	[34]
Multiwalled CNTs	313	55	[35]
Coffee waste	298	63	[36]
Al-CNTs	298	70	[37]
PANI-coated fiber	298	76	[38]
Protonated chitosan	293	89	[39]
Ni-polymer	298	125	[40]
Glycerol-LDH	298	444	[41]
Labeo rohita fish scale	283	520	This work

3.2.7 Temperature effect and thermodynamic study

The adsorption phenomenon with respect to temperature is investigated, and thermodynamic parameters, such as standard Gibbs-free energy change (ΔG^0), standard enthalpy change (ΔH^0), and standard entropy change (ΔS^0), are determined from the slope and intercept (Fig. 5c) based on the assumption that the active coefficient of the solutes added in solution is unity (Eqs. 7–9) [42]. The obtained data for the sorption of MO-H is given in Table 5.

Table 5 Parameters obtained from the thermodynamic analyses for MO-H adsorption on scale at *pH* 5.3 (± 0.1)

Temperature	K_F	ΔG^0 (kJ mol^{-1})	ΔH^0 (kJ mol^{-1})	ΔS^0 (kJ mol^{-1} K^{-1})
283K	2.541	−0.953	−9.175	0.029
303K	1.278	−0.466		
323K	0.833	−0.021		

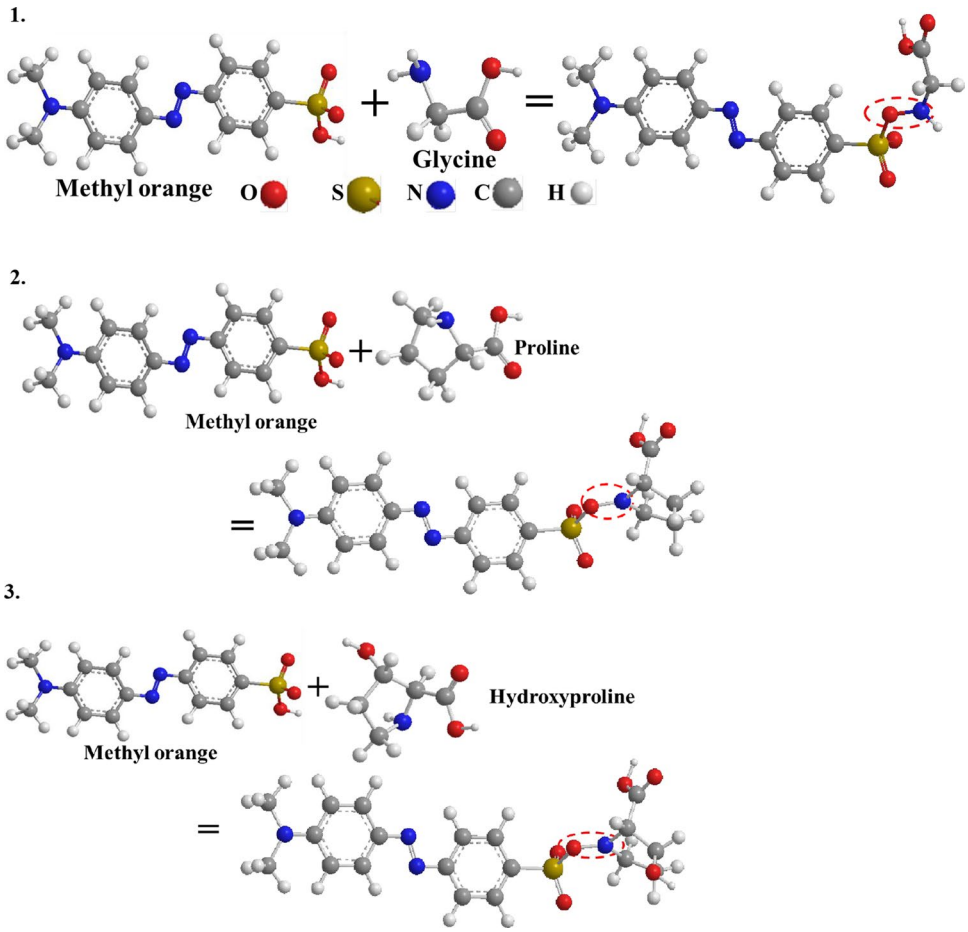

Fig. 6 3D interaction of MO^- with glycine (1), proline (2), and hydroxyproline (3) in acid medium

The negative ΔG^0 values indicate that the process is spontaneous. It is also evident from Table 5 that the ΔG^0 values gradually increase with the increasing temperature of the reaction mixture, which signifies that the adsorption process gradually diminishes with rising temperature. Thus, the adsorbent is more efficient at lower temperatures. The negative ΔH^0 describes the process as exothermic, whereas at higher temperatures, the adsorption is dropped, agreeing with the La Chattelier's principle. The + ΔS^0 indicates the greater affinity of fish scale in aqueous solution with an increase in degrees of freedom at the interface. The randomness at the interface of solid-liquid is presumably due to the release of hydrated molecules replacing MO^-. From the lower negative value of ΔH^0, it is clear that the adsorption is exothermic and corroborated by the physisorption type reaction as revealed by the mechanism study [21].

3.2.8 Adsorption mechanism

Fish scale contains huge amount of useful materials, including collagens fat, vitamins, and inorganic compounds. Interestingly, collagen contains essential proteins in organisms. The carboxyl groups and amino functionalities in these compounds trigger the adsorption process of MO-H. Below *pH* 7, the C-terminal amino acids of protein are stabilized by H^+ ions, and consequently, the cationic N-terminal takes part in interacting with the sulfur and oxygen center of methyl orange. The glycine, proline, and hydroxyproline are the three major amino acids in fish collagen as reported before [43]. Figure 6 shows the electrostatic interaction between sulfonate group (R-SO_3^-) of methyl orange and $-NH_2$ and > NH groups of amino acids (glycine, proline, and hydroxyproline) of biosorbent fish scale.

4 Conclusions

The fish scale, a bio-waste material, was successfully used to clean dye-contaminated water. Results indicate a remarkable removal efficiency of biosorbent (Langmuir capacity 520 mg g^{-1}, 283 K) for MO-H dye. Response surface methodology and ANOVA optimize the variable parameter ranges and prove the order of their influence as *Ce* > *T* > *pH* on adsorption process. The optimum conditions of *pH*, concentration of MOH, and temperature are observed to be 5.3 (± 0.1), 200 mg/L, and 283 K, respectively. At *pH*~5.3, the color removal

% increases (~94%) with increasing adsorbent dose and contact time. The best fit of the Freundlich isotherm model indicates multilayer adsorption on a scale surface. On the fish scale, MO-H adsorption is exothermic ($\Delta H^0 = -9.175$ kJ mol^{-1}) and entropically favorable ($\Delta S^0 = +0.029$ kJ mol^{-1} K^{-1}). The lower value of ΔH^0 indicates the physisorption nature of adsorption. The adsorption mechanism demonstrates the affinity of dye towards proteins such as proline, hydroxyproline, glycine, etc. available in fish scale biosorbent. The sulphonate group ($R\text{-}SO_3^-$) of methyl orange takes part in binding interactions with the $-NH_2$ and $^>$ NH groups of amino acids, such as glycine, proline, and hydroxyproline.

Supplementary Information The online version contains supplementary material available at https://doi.org/10.1007/s13399-022-02614-x.

Acknowledgements D. Nandi sincerely acknowledges KMUTNB, Bangkok 10800, for funding and research facility (contract no.: KMUTNB-Post-65-02) Also, Sabarish Radoor, KMUTNB, Bangkok 10800, is acknowledged for his support.

Code availability Not applicable

Author contribution DN, investigation, formal analysis, and writing; HP and JP, conceptualization, methodology, and investigation; Suchart Siengchin, supervision, project administration, resources, and funding acquisition.

Data availability Not applicable

Declarations

Ethics approval Not applicable

Consent to participate Not applicable

Consent for publication Not applicable

Conflict of interest The authors declare no competing interests.

Author statement All study is made by the corresponding author.

References

1. Pradhan SS, Konwar K, Ghosh TN et al (2020) Multifunctional iron oxide embedded reduced graphene oxide as a versatile adsorbent candidate for effectual arsenic and dye removal. Colloid Interf Sci Commun 39(100319):1–7
2. Al-Tohamy R, Ali SS, Li F et al (2022) A critical review on the treatment of dye-containing wastewater: ecotoxicological and health concerns of textile dyes and possible remediation approaches for environmental safety. Ecotoxicol Environ Saf 231(113160):1–17
3. Raj A, Mandal J, Golui D et al (2021) Determination of suitable extractant for estimating plant available arsenic in relation to soil properties and predictability by solubility-FIAM. Water Air Soil Pollut 232(247):1–11
4. Pagga UM, Taeger K (1994) Development of a method for adsorption of dyestuffs on activated sludge. Water Res 28(5):1051–1057
5. Crini G, Badot PM (2008) Application of chitosan, a natural aminopolysaccharide, for dye removal from aqueous solutions by adsorption processes using batch studies: a review of recent literature. Prog Polym Sci 33:399–347
6. Thite VD, Giripunje SM (2022) Adsorption and photocatalytic performance of ZnAl layered double hydroxide nanoparticles in removal of methyl orange dye. Nanotechnol Environ Eng 7:1–10. https://doi.org/10.1007/s41204-021-00186-1
7. Maruthanayagam A, Mani P, Kaliappan K et al (2020) In vitro and in silico studies on the removal of methyl orange from aqueous solution using Oedogonium subplagiostomum AP1. Water Air Soil Pollut 231(232):1–21
8. Jadhav SA, Garud HB, Patil AH et al (2019) Recent advancements in silica nanoparticles based technologies for removal of dyes from water. Colloid Interf Sci Commun 30(100181):1–12
9. Bazan-Aguilar A, López EO, Ponce-Vargas M (2021) Biomass-based carbon electrodes in the design of supercapacitors: an electrochemical point of view. IntechOpen. https://doi.org/10.5772/intechopen.97649
10. Niero G, Corrêa AXR, Trierweiler G et al (2019) Using modified fish scale waste from Sardinella brasiliensis as a low-cost adsorbent to remove dyes from textile effluents. J Environ Sci Health A Tox Hazard Subst Environ Eng 54(11):1083–1090
11. Chakraborty J, Dey S, Halder UC (2016) An eco-friendly biosorbent derived from fish (Carp) scale: a study of commercial dye removal. Int J Sci Eng Res 7:72–76
12. Paul Das M, Renuka M, Vijaylakshmi JV (2018) Removal of methylene blue by adsorption using fish scale chitin. Nat Environ Pollut Technol 17:993–998
13. Islam MA, Hameed BH, Ahmed MJ et al (2022) Porous carbon–based material from fish scales for the adsorption of tetracycline antibiotics. Biomass Conv Bioref. https://doi.org/10.1007/s13399-021-02239-6
14. Chowdhury S, Das Saha P, Ghosh UC (2012) Fish (*Labeo rohita*) scales as potential low-cost biosorbent for removal of malachite green from aqueous solutions. Bioremediat J 16:235–242
15. Tamás MJ, Sharma SK, Ibstedt S et al (2014) Heavy metals and metalloids as a cause for protein misfolding and aggregation. Biomolecules 4(1):252–267
16. IARC working group on the evaluation of carcinogenic risks to humans. Some aromatic amines, organic dyes, and related exposures. Lyon (FR): International Agency for Research on Cancer; 2010. (IARC) Monographs on the evaluation of carcinogenic risks to humans, no. 99.) General introduction to the chemistry of dyes. https://www.ncbi.nlm.nih.gov/books/NBK385442
17. Nandi D, Basu T, Debnath S et al (2013) Mechanistic insight for the sorption of Cd(II) and Cu(II) from aqueous solution on magnetic Mn-doped Fe(III) oxide nanoparticle implanted graphene. J Chem Eng Data 58(10):2809–2818
18. O'Mahony T, Guibal E, Tobin JM (2002) Reactive dye biosorption by Rhizopus arrhizus biomass. Enzyme Microb Technol 31:456–463
19. Nandi D, Gupta K, Ghosh AK et al (2012) Manganese-incorporated iron(III) oxide–graphene magnetic nanocomposite: synthesis, characterization, and application for the arsenic(III)-sorption from aqueous solution. J Nanopart Res 14(1272):1–14
20. Freundlich HMF (1906) Over the adsorption in solution. J Phys Chem 57:385–471
21. Redlich O, Peterson DL (1959) A useful adsorption isotherm. J Phys Chem 63:1024–1026
22. Nandi D, Saha I, Ray SS et al (2015) Development of a reduced-graphene-oxide based superparamagnetic nanocomposite for the removal of nickel (II) from an aqueous medium via a fluorescence sensor platform. J Colloid Interf Sci 454:69–79

23. Wu Q, Liang H, Li M et al (2016) Hierarchically porous carbon membranes derived from PAN and their selective adsorption of organic dyes. Chinese J Polym Sci 34:23–33
24. Hadi P, Yeung KY, Barford J et al (2015) Significance of effective surface area of activated carbons on elucidating the adsorption mechanism of large dye molecules. J Environ Chem Eng 3:1029–1037
25. Sripriya R, Kumar R (2015) A novel enzymatic method for preparation and characterization of collagen film from swim bladder of fish rohu (labeo rohita). Food Nutr Sci 6:1468–1478
26. Poy H, Lladosa E, Gabaldón C et al (2021) Optimization of rice straw pretreatment with 1-ethyl-3-methylimidazolium acetate by the response surface method. Biomass Convers Biorefin. https://doi.org/10.1007/s13399-021-02111-7
27. Nandi D, Ghosh SK, Ghosh A et al (2021) Arsenic removal from water by graphene nanoplatelets prepared from nail waste: a physicochemical study of adsorption based on process optimization, kinetics, isotherm and thermodynamics. Environ Nanotechnol Monit Manag 16(100564):1–11
28. Vinoth M, Lim HY, Xavier R et al (2010) Removal of methyl orange from solutions using yam leaf fibers. Int J ChemTech Res 2(4):1892–1900
29. Buema G, Trifas LM, Harja M (2021) Removal of toxic copper ion from aqueous media by adsorption on fly ash-derived zeolites: kinetic and equilibrium studies. Polymers 13(3468):1–14
30. Allen SJ, McKay G, Khader KYH (1989) Intraparticle diffusion of a basic dye during adsorption onto sphagnum peat. Environ Pollut 56:39–50
31. Robati D, Mirza B, Rajabi M (2016) Removal of hazardous dyes-BR 12 and methyl orange using graphene oxide as an adsorbent from aqueous phase. Chem Eng J 284:687–697
32. Datta D, Kerkez O, Kuyumcu SS (2017) Adsorptive removal of malachite green and Rhodamine B dyes on Fe3O4/activated carbon composite. J Dispers Sci Technol 38:1556–1562
33. Mogaddasi F, Momen Heravi M, Bozorgmehr MR et al (2010) Kinetic and thermodynamic study on the removal of methyl orange from aqueous solution by adsorption onto camel thorn plant. Asian J Chem 22(7):5093–5100
34. Córdova BM, Santa Cruz JP, Ocampo T, Huamani-Palomino RG, Baena-Moncada AM (2020) Simultaneous adsorption of ternary mixture of brilliant green, Rhodamine B and methyl orange as artificial wastewater onto biochar from cocoa pod husk waste. Quantification of dyes using the derivative spectrophotometry method. New J Chem 44:8303–8316
35. Zhao D, Zhang W, Chen C (2013) Adsorption of methyl orange walled carbon nanotubes. Procedia Environ Sci 18:890–895
36. Lafi R, Hafiane A (2016) Removal of methyl orange (MO) from aqueous solution using cationic surfactants modified coffee waste (MCWs). J Taiwan Inst Chem Eng 58:424–433
37. Kang DJ, Yu XL, Ge MF et al (2017) Novel Al-doped carbon nanotubes with adsorption and coagulation promotion for organic pollutant removal. J Environ Sci 54:1–12
38. Herrera MU, Futalan CM, Gapusan R et al (2018) Removal of methyl orange dye and copper (II) ions from aqueous solution using polyaniline-coated kapok (Ceiba pentandra) fibers. Water Sci Technol 78(5):1137–1147
39. Huang R, Liu Q, Huo J et al (2017) Adsorption of methyl orange onto protonated cross-linked chitosan. Arab J Chem 10:24–32
40. Cheng HJ, Ma YS, Yuan RX (2018) Synthesis, structure and adsorption studies of a nickel coordination polymer with selective removal on methyl orange. Inorganica Chim Acta 476:1–6
41. Yao W, Yu S, Wang J et al (2017) Enhanced removal of methyl orange on calcined glycerol-modified nanocrystallined Mg/Al layered double hydroxides. Chem Eng J 307:476–486
42. Pla-Franco J, Lladosa E, Loras S et al (2014) Thermodynamic analysis and process simulation of ethanol dehydration via heterogeneous azeotropic distillation. Ind Eng Chem Res 53:6084–6093
43. Jafari H, Lista A, Siekapen MM (2020) Fish collagen: extraction, characterization, and applications for biomaterials engineering. Polymers 12:2230